The central spindle drives anaphase chromosome segregation

Geng-Yuan Chen[1], Changfeng Deng[2], David M. Chenoweth[2], Michael A. Lampson[1]

[1]Department of Biology, University of Pennsylvania, Philadelphia, PA, 19104
[2]Department of Chemistry, University of Pennsylvania, Philadelphia, PA, 19104

Categories: Cell Biology, Anaphase

Keywords: chromosome segregation, spindle mechanics, chemical optogenetics

Abstract

Anaphase chromosome segregation depends on forces exerted by spindle microtubules. In the current model, forces on chromosomes are mediated through the spindle poles: sliding of antiparallel microtubules in the central spindle pushes poles apart, while kinetochore microtubule (kMT) depolymerization pulls chromosomes towards the poles. Here we show that the central spindle is directly linked to the chromosomes rather than the poles in anaphase, based on three lines of evidence. Chromosomes in monopolar spindles can move away from the pole, consistent with forces exerted by antiparallel microtubule sliding. In bipolar spindles, kMT depolymerization is constrained by suppressing central spindle sliding, indicating kinetochore linkage to the central spindle. Finally, increasing the rate of kMT depolymerization slows pole separation without increasing chromosome separation velocity. We conclude that central spindle sliding drives anaphase chromosome separation, while kMT depolymerization limits spindle elongation.

Introduction

During cell division, sister chromosomes segregate in anaphase to partition the two replicated genomes into daughter cells. Three mechanisms of force generation in anaphase have been described. First, kinetochore microtubule (kMT) bundles depolymerize to pull chromosomes and spindle poles towards each other. Second, antiparallel microtubule sliding in the central spindle pushes the two half-spindles apart. Third, astral microtubules pull spindle poles apart. According to the current model (referred to here as the “pole-linked” model), these forces act to separate chromosomes via spindle poles (**Figure 1**) (*1*). Antiparallel microtubule sliding and astral microtubules combine to push and pull the poles apart and elongate the spindle (termed anaphase B) (*2, 3*). As the poles separate, kMT depolymerization pulls each chromosome towards its attached pole (anaphase A) (*4, 5*). Experimental observations supporting all three force-generating mechanisms are consistent with the pole-linked model but do not rule out an alternative “chromosome-linked” model. If the central spindle links to chromosomes rather than poles, for example by parallel crosslinkers between kMTs and central spindle microtubules, then antiparallel sliding can directly separate chromosomes (*6, 7*). In this model, forces exerted by kMT depolymerization and astral microtubules pull on poles to regulate spindle elongation but are not necessary for chromosome separation.

We designed three assays to distinguish between the pole-linked and chromosome-linked models. First, we examined anaphase chromosome motions on monopolar spindles (**Figure 2A**) (*8*), in which either one or both kinetochores of a sister pair attach to the single pole (*9*). The pole-linked model predicts poleward motions for pole-attached chromosomes because forces on chromosomes are directed towards the poles via kMTs, or no motions for chromosomes that are detached from the pole. In contrast, the chromosome-linked model predicts that antiparallel sliding can move chromosomes away from the pole, depending on the arrangement of antiparallel bundles marked by the antiparallel microtubule crosslinker PRC1 (Protein Regulator of Cytokinesis 1) (*10*) (**Figure 2B, Videos 1-2**). For some kinetochores, kMTs are oriented away from the pole (*11*) and can link to these antiparallel bundles to generate anti-poleward forces. Second, we measured rates of kMT depolymerization after suppressing antiparallel sliding in the central spindle. In the pole-linked model, kMT plus-ends are not linked to the central spindle, so antiparallel sliding should be uncoupled from kMT depolymerization. In the chromosome-linked model, kMT plus and minus ends are linked to the central spindle and the poles, respectively, so kMT depolymerization is constrained by the relative rates of central spindle sliding and pole separation (**Figure 1**). Third, we increased the rate of kMT depolymerization and measured kinetochore separation and pole separation velocities. The pole-linked model predicts increased kinetochore separation velocity with no effect on pole separation. Alternatively, the chromosome-linked model predicts no effect on kinetochore separation but slowed pole separation, as kMT depolymerization pulls poles towards the chromosomes (*6*) (**Figure 1**).

Results

For the first assay, we initiated anaphase on monopolar spindles by inhibiting the spindle assembly checkpoint using a photocaged inhibitor of the checkpoint kinase MPS1 (Monopolar Spindle 1) (**Figure 2C**) (manuscript in preparation). This inhibitor is linked to the Halo ligand and therefore binds covalently to the Halo-tagged kinetochore anchor SPC25. MPS1 is inhibited only after uncaging with a pulse of light. As the inhibitors are bound to SPC25 and do not diffuse between cells, anaphase can be induced in one cell at a time by local uncaging. This chemical optogenetic approach allows sequential live imaging of individual cells with high temporal resolution. After MPS1 inhibition, we find that PRC1 signals gradually decrease in length and increase in intensity, indicating antiparallel sliding that decreases the overlap length in each bundle (**Figure S1**), as observed in the central spindle in normal bipolar anaphase (*12-14*) and in reconstituted systems (*15, 16*). We analyzed kinetochore motions separately for sister pairs either colocalized to (on-bundle) or away from (off-bundle) PRC1 signals (**Figure 2D-F**). Off-bundle pairs exhibit minimal movement of sisters away from each other, consistent with a lack of anti-poleward forces. Conversely, some on-bundle sisters move apart, with the distal kinetochore of these pairs moving away from the pole (**Figure 2G**). This result is consistent with the chromosome-linked model, in which antiparallel sliding drives chromosome movements. Previous findings, in which sister

kinetochores separate after detaching a kinetochore from one pole of a bipolar spindle by laser ablation, are also consistent with the chromosome-linked model (*17*).

For the second and third assays, we manipulated specific microtubule populations within bipolar spindles using another chemical optogenetic approach. We used a photocaged small molecule that heterodimerizes HaloTag and *Escherichia coli* dihydrofolate reductase (eDHFR) fusion proteins (**Figure 3A**) (*18, 19*). This approach provides temporal precision by light activation and molecular specificity by using genetically tagged constructs (*20*). By activating immediately after anaphase onset, our manipulations do not affect earlier stages of spindle formation and kinetochore attachment.

To generate "brake" complexes that suppress antiparallel sliding for the second assay, we fused HaloTag to full-length dimeric PRC1 (the anchor) and fused eDHFR to a monomeric PRC1 truncation mutant (PRC1M, the effector) that binds to microtubules without crosslinking activity on its own. Uncaging recruits PRC1M to dimeric PRC1 bound to antiparallel bundles, which strengthens PRC1 binding to microtubules and thus increases friction to suppress sliding within the bundle (**Figure 3B-C**). Before activation, PRC1M binds to microtubules proportional to local microtubule density, with a subtle enrichment around the equator (**Figure 3D, Video 3**). This enrichment increases after activation, consistent with recruitment to PRC1-labeled antiparallel bundles in the central spindle (*14*). To determine the effects of activation on kinetochore and pole movements and on kMT depolymerization, we measured three distances at each time frame: between separating kinetochores, between poles, and between kinetochores and their attached pole (**Figure 3E**). We fit a slope to the earliest time window exhibiting a linear range for all distances (**Figure 3F**). Formation of brake complexes decreases separation velocities for both poles (V_{PP}) and kinetochores (V_{KK}), indicating suppressed bundle sliding (**Figure 3G-H**). Reduced kMT depolymerization (V_{PK}) after braking (**Figure 3I**) indicates that both kMT ends are constrained, as predicted by the chromosome-linked model. Consistent with this result, previous findings showed that inhibiting antiparallel sliding motors reduces kMT depolymerization (*21, 22*).

For the third assay, we recruited the microtubule depolymerase MCAK (kinesin-13) to kinetochores to increase the rate of kMT depolymerization (**Figure 4A-B**) (*23*). As MCAK is active only at microtubule ends (*24*), recruitment to kinetochores increases depolymerization of kMTs but not other proximal microtubules. We first tested this assay in metaphase spindles, in which cohesion prevents sister kinetochores from moving farther apart. We find that MCAK recruitment leads to spindle shortening, as kMT depolymerization pulls poles inward towards the kinetochores (**Figure 4C-D, Video 4**). To test the effects of increasing kMT depolymerization in anaphase, we recruited MCAK to kinetochores within 1 min after sister kinetochores start to move apart, indicating anaphase onset (**Figure 4E-F, Video 5**). We measured kinetochore and pole velocities and kMT depolymerization as in **Figure 3E-F**. MCAK recruitment increases the rate of kMT depolymerization (**Figure 4G**), as expected, but does not increase kinetochore separation velocity (**Figure 4H**). Instead, pole separation velocity decreases (**Figure 4I**), indicating that poles are pulled inward towards the kinetochores as in metaphase

(**Figure 4C-D**). These results indicate that kinetochores are linked to the central spindle, so that antiparallel sliding moves chromosomes apart while kMT depolymerization regulates spindle elongation, consistent with the chromosome-linked model.

Discussion

By manipulating spindle organization and specific microtubule populations within the spindle, our experiments distinguish between the two mechanical models for anaphase chromosome segregation. The results of all three assays are consistent with the chromosome-linked model. First, antiparallel sliding can separate sister chromosomes on monopolar spindles by moving the distal kinetochore away from the pole (**Figure 2**). Second, suppressed antiparallel sliding slows kMT depolymerization, indicating that kinetochores are linked to the central spindle (**Figure 3**). Third, enhanced kMT depolymerization slows pole separation but does not affect kinetochore separation (**Figure 4**). Previous findings, including in other model systems such as *C. elegans* oocytes and embryos and *Xenopus* egg extracts, are also consistent with the chromosome-linked model: antiparallel sliding velocity within the central spindle matches kinetochore separation velocity in anaphase, and laser ablation of the central spindle between sister kinetochores either slows or transiently halts kinetochore separation (*17, 22, 25-27*). Furthermore, kinetochores continue to separate after ablating microtubules midway between kinetochores and their attached poles (*25*), and reduced braking in antiparallel bundles by PRC1 depletion increases chromosome segregation velocities (*13*). These findings indicate that antiparallel sliding in the central spindle directly moves chromosomes. The central spindle also pushes the poles apart, and we propose that depolymerizing kMTs pull poles inward towards the kinetochores to restrict spindle elongation. Consistently, in *C. elegans* meiosis, spindle length decreases even with antiparallel sliding in the central spindle, suggesting that kMT depolymerization pulls poles inwards (*28*).

Our findings suggest that microtubule bundles in the central spindle couple to kinetochore-proximal regions of kMTs, since enhanced kMT depolymerization at the kinetochore does not increase kinetochore separation velocity (**Figure 4**). Consistently, kMTs are close to central spindle microtubules in EM images (*25*), and kMT deformation by microneedle manipulation suggests crosslinking to the central spindle near chromosomes (*29*). For sister chromosomes to move in opposite directions, we propose that coupling is mediated by parallel crosslinkers or branching microtubule arrays so that chromosomes move with the pole to which they are attached (*3, 30*). Before anaphase, short microtubules bind kinetochores at their plus-ends, while the minus-ends interact with antiparallel bundles in the central spindle (*31*). Minus-end directed motors sort these nascent kMTs and establish parallel coupling to central spindle microtubules to biorient sister kinetochores (**Figure S2A**) (*32*). Alternatively, parallel microtubule arrays can assemble by growing microtubules from existing microtubule templates (*33, 34*). Microtubules nucleated from sister kMTs can thus grow inward to generate a “bridging-fiber” by antiparallel crosslinking (**Figure S2B**) (*17, 35*). Furthermore, our model suggests that parallel couplers bind the central spindle to kMTs tightly to move them, while also maintaining the coupling as kMTs depolymerize at the

kinetochore. Couplers may bind tightly to the kMT lattice but weakly at the depolymerizing tip, thus releasing from the depolymerizing tip and capturing a straight lattice nearby, similar to models for maintaining kinetochore attachment to depolymerizing microtubule tips (*4*).

Restricting spindle elongation by kMT depolymerization may be important for later stages of division. Increased spindle elongation is associated with midzone buckling and defocused cytokinetic furrows (*12-14, 36, 37*). In addition, spindle poles act as hubs for numerous biochemical and mechanical cues (*38-40*), so restricted spindle elongation may regulate pole communication with spindle midbodies or the cytokinetic furrow. Hence, telophase biology likely requires coordination between pole and chromosome separation velocities via depolymerizing kMTs.

Materials and Methods

Synthesis, characterization, and storage of chemical optogenetic probes. The photoactivatable dimerizer (CTH) (*19, 23*) and photoactivatable localized MPS1 inhibitor (NRH, manuscript in preparation) were prepared as previously described. Both compounds were dissolved in DMSO at 20 mM and stored as 1 μL aliquots in amber plastic microcentrifuge tubes at -80 °C.

Small molecule inhibitors. All stocks were dissolved in DMSO and stored at -20 °C. Stock concentrations include 20 mM S-Trityl-L-Cysteine (STLC, Eg5 inhibitor; Sigma Aldrich), 10 mM Verapamil (Tocris), and 100 μM GSK-923295 (CenpE rigor inhibitor; MedChemExpress). Fresh aliquots were used for all experiments.

Plasmids. The pEM705 backbone with a CAG promoter was used to clone all plasmids for anchors and effectors (*41*). The kinetochore anchor SPC25, fused to three tandem copies of HaloTag and an eGFP on its N-terminus (3×Halo-GFP-SPC25), was used as previously described (*19, 23*). To manipulate central spindle mechanics, PRC1 was used as an anchor, fused to 3× HaloTag with the far-red fluorescent reporter, miRFP670nano3 (hereafter denoted 670nano3), on its N-terminus (3×Halo-670nano3-PRC1).

All effectors were designed based on the construct with the red fluorescent protein mScarlet fused to the N terminus of *Escherichia coli* dihydrofolate reductase DHFR (mScarlet-eDHFR). For targeted microtubule depolymerization, the phospho-resistant motor domain of human MCAK ($MCAK_{179\text{-}583;S192A}$) was fused to the N terminus of mScarlet-eDHFR (MCAK-mScarlet-eDHFR) (*23, 42*). To suppress microtubule sliding, a monomeric PRC1 mutant (PRC1M, $PRC1_{341\text{-}620}$) (*43*) was fused to the C terminus of mScarlet-eDHFR to make mScarlet-eDHFR-PRC1M.

To label spindle poles, a single copy or two tandem copies of the PACT (Pericentrin and AKAP Centrosome Targeting) (*44*) domain was fused to eGFP (PACT-GFP or 2×PACT-GFP) in the pcDNA3.1 backbone containing cytomegalovirus and T7 promoters. To label the central spindle, full-length PRC1 was fused to two tandem copies of 670nano3 (2×670nano3-PRC1), using pEM705 as the backbone.

Cell cultures and transfection. HeLa RMCE (recombination-mediated cassette exchange) acceptor cells were passaged at 37°C in the growth medium containing DMEM (Gibco) supplemented with 10% Fetal Bovine Serum (Clontech) and 1% penicillin/streptomycin (Life Technologies), within 5% CO_2 atmosphere and humidity. For assays, cells were cultured on coverslips (Bellco) coated by poly-D-lysine (Sigma-Aldrich) for at least 16 h, and then transfected with the desired constructs using Lipofectamine 3000 (Invitrogen) in Opti-MEM (Gibco) for at least 24 h.

Manipulations of mechanics and biochemistry at kinetochores were conducted with cells stably expressing 3×Halo-GFP-SPC25, as previously described (*19, 23*). For the monopolar anaphase assay, cells were transfected with 0.5-1 μg 2×670nano3-PRC1 and 250 ng PACT-GFP to mark the central spindle and spindle poles, respectively. For kMT depolymerization, cells were transfected with 1-1.5 μg MCAK-mScarlet-eDHFR and 250 ng 2×PACT-GFP.

Manipulations of central spindle mechanics were conducted with cells transiently transfected with 0.6 μg Scarlet-eDHFR-PRC1M and 0.6 μg 3×Halo-670nano3-PRC1, together with 100 ng CenpB-GFP and 250 ng 2×PACT-GFP for labeling centromeres and poles, respectively.

Photoactivation and dimerization. For recruitment experiments, cells were placed in a magnetic chamber (Chamlide CM-S22-1; LCI) and incubated with growth medium and CTH for 1 h. Unbound CTH was washed out by incubating for 20 min in imaging medium containing L15 without phenol red (Gibco) (imaging medium) plus 10% FBS and 1% penicillin/streptomycin. The medium was then replaced with fresh imaging medium, and the chamber was moved to a stage in a 37°C environmental chamber (PeCon). For dimerization experiments, cells were imaged live to determine the time of anaphase onset. CTH was activated within 1 min after sister kinetochores start to move apart, using a 405-nm laser (CrystaLaser LC) controlled by iLas2 software (Roper Scientific) installed on MetaMorph (Molecular Devices), as previously described (*23*). Activation was performed over the entire cell at 25% laser power with 5 repetitions. To induce anaphase in monopolar cells, cells were incubated with 10 μM Verapamil (an efflux pump inhibitor) and 20 μM STLC in growth medium for 2 h, then 20 μM NRH was added for 1 h. Unbound NRH was washed out by incubating in imaging medium with STLC for 30 min. NRH was uncaged by a 5-second light pulse using a mercury arc lamp filtered at 385/11 nm, and imaging started 15-20 min later. Procedures with light-sensitive molecules were performed under red light in the room.

Image acquisition. Fixed or live cells at 37 °C were imaged with a confocal microscope (DM4000; Leica), equipped with a 100× 1.4 NA oil immersion objective (Leica), an XY Piezo-Z stage (Applied Scientific Instrumentation), a CSU10 spinning disk (Yokogawa), an electron multiplier charge-coupled device camera (ImageEM; Hamamatsu Photonics), and a 4-line laser module (405 nm, 488 nm, 561 nm, and 639 nm; Vortran Stradus VersaLase 4), as previously described (*23*). Images were acquired with a 10-60s time interval, with 0.5-2 μm spacing for z-stacks covering 6-15 μm total.

Data analyses and statistical tests.

For monopolar anaphase cells, both kinetochores and poles were tracked by the Fiji::MTrackJ plug-in. In each frame, the distances of two sisters relative to the pole were calculated (D_{PK}). The distance difference between the two sisters (ΔD_{PK}) represents the inter-kinetochore distance along the axis between the pole and kinetochores (D_{KK}). For each trajectory, the maximum kinetochore separation velocity (max V_{KK}) represents the maximal displacement of inter-kinetochore distance (D_{KK}) across all possible one-minute time windows. A cutoff was defined as the 95% percentile of max V_{KK} of off-bundle sister kinetochore pairs.

For bipolar anaphase cells, the coordinates of kinetochores and spindle poles were measured by the Fiji::TrackMate and Manual Tracking plug-ins, respectively. Kinetochore coordinates were projected to the mitotic axis defined by poles, and then grouped based on their closest pole. In each frame, the median position of each group represents the centroid of projected kinetochores. Initial velocities were defined by the time window exhibiting linear displacement between the two poles (V_{PP}), between the two kinetochore centroids (V_{KK}), and between a kinetochore centroid and its corresponding pole ($-V_{PK}$).

Data from measurements were analyzed by MATLAB. Two-tailed Student's t-test were used to compare measurements between groups.

Acknowledgments: We thank the Philly ChromoClub and the Penn Center for Genome Integrity for discussions. This work was supported by the NIH (GM122475 and P01-CA265794) and the Basser Center for BRCA.

Author contributions: GYC designed and conducted cell biology experiments and wrote the manuscript. CD and DMC synthesized and characterized chemical optogenetic probes. MAL designed experiments and edited the manuscript.

Competing interests declaration: The authors claim no competing financial interests.

Data sharing plan and availability. The datasets generated and analyzed during the current study are available from the corresponding author on reasonable request without restriction.

Materials and Correspondence. Cell lines, chemicals, and protocols are available upon request. The corresponding authors adhere to the NIH Grants Policy and Sharing of Unique Research Resources. Correspondence and requests for materials should be addressed to MAL (lampson@sas.upenn.edu).

Supplementary Information is available for this paper.

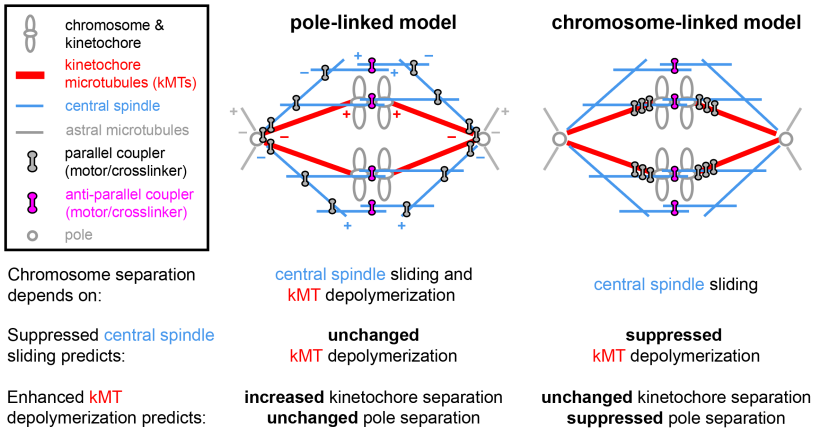

Figure 1. Mechanical models for anaphase chromosome segregation. Spindle microtubules exhibit polarity, with minus-ends (-) and plus-ends (+) facing toward and away from poles, respectively. Parallel couplers (gray dumbbells) crosslink parallel microtubule arrays (blue) to form two half-spindles, while antiparallel couplers (magenta dumbbells) in the central spindle slide the two half-spindles apart. Astral microtubules (gray) pull poles outwards by cortical force generators (not shown). Depolymerizing kMTs (red) pull poles and chromosomes towards each other. In the pole-linked model, the central spindle links to spindle poles, so that antiparallel sliding pushes poles apart while kMT depolymerization pulls sister chromosomes toward poles. In the chromosome-linked model, the central spindle links to kMTs near chromosomes, so that antiparallel sliding directly moves sister chromosomes apart. Predictions of suppressed central spindle sliding and enhanced kMT depolymerization are shown (see text for details).

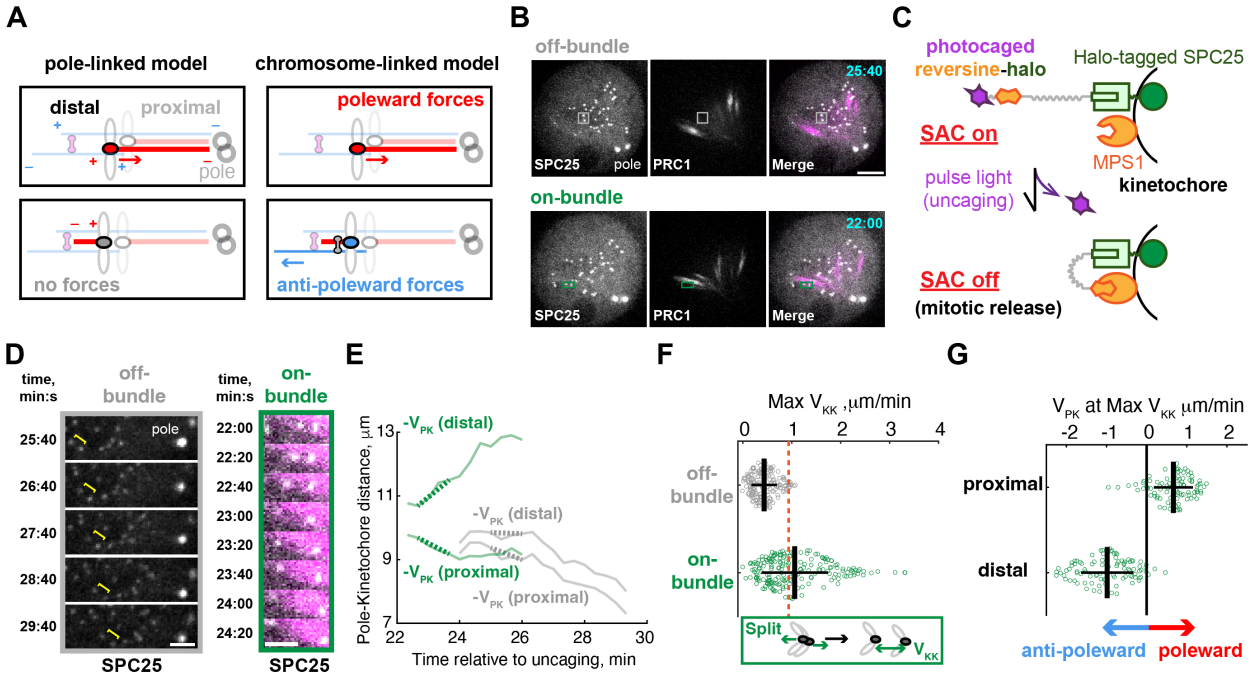

Figure 2. Anti-poleward kinetochore motions in monopolar anaphase. (A) Both mechanical models predict poleward motions of kinetochores that are attached to the pole, due to depolymerization of kMTs. The two models predict different motions for the distal kinetochore if its kMTs are oriented away from the pole. In the pole-linked model, no forces are exerted on the distal kinetochore in anaphase. In the chromosome-linked model, antiparallel sliding can exert anti-poleward force if the distal kinetochore links to an antiparallel bundle. **(B-D)** Monopolar anaphase assay. Representative images (B) show cells expressing Halo-GFP-SPC25 (kinetochores), PACT-GFP (spindle poles), and 670nano3-PRC1 (antiparallel bundles), incubated with the kinesin-5 inhibitor STLC to create monopolar spindles. Schematic (C) illustrates the chemical optogenetic approach for spindle checkpoint silencing in single cells. The MPS1 inhibitor (reversine, orange) is linked to a photocage (purple) and a Halo ligand (green). The caged inhibitor localizes to kinetochores by binding to the Halo-tagged kinetochore protein SPC25 and inhibits MPS1 only after uncaging. Time-lapse images (D) show representative sister kinetochore pairs localized away from or close to antiparallel bundles (off-bundle or on-bundle, respectively), boxed in B. Yellow line: distance between the off-bundle sisters; time stamps (min:s): time after uncaging at t=0. **(E)** Individual kinetochore movements relative to the pole for the off-bundle (grey) and on-bundle (green) sister pairs shown in D. Kinetochore velocity relative to the pole (V_{PK}) was calculated as the displacement within a one-minute time window, with poleward motion defined as the positive direction. Dashed lines represent the maximal velocity of sister kinetochore separation (Max V_{KK}). **(F)** Max V_{KK} plotted for off-bundle (n=168) and on-bundle (n=204) sister kinetochore pairs. Orange dashed line: upper bound for pairs that behave as off-bundle (95th percentile of the Max V_{KK} distribution for off-bundle pairs). Some on-bundle pairs separate with high V_{KK} as shown in E (green traces). **(G)** For each on-bundle pair with Max V_{KK} above the orange line (n=93 pairs), indicating functional interactions with the

bundle, V_{PK} is plotted for the proximal and distal sisters. Black lines: mean ± SD. Scale bars, 5 μm in C or 2 μm in D.

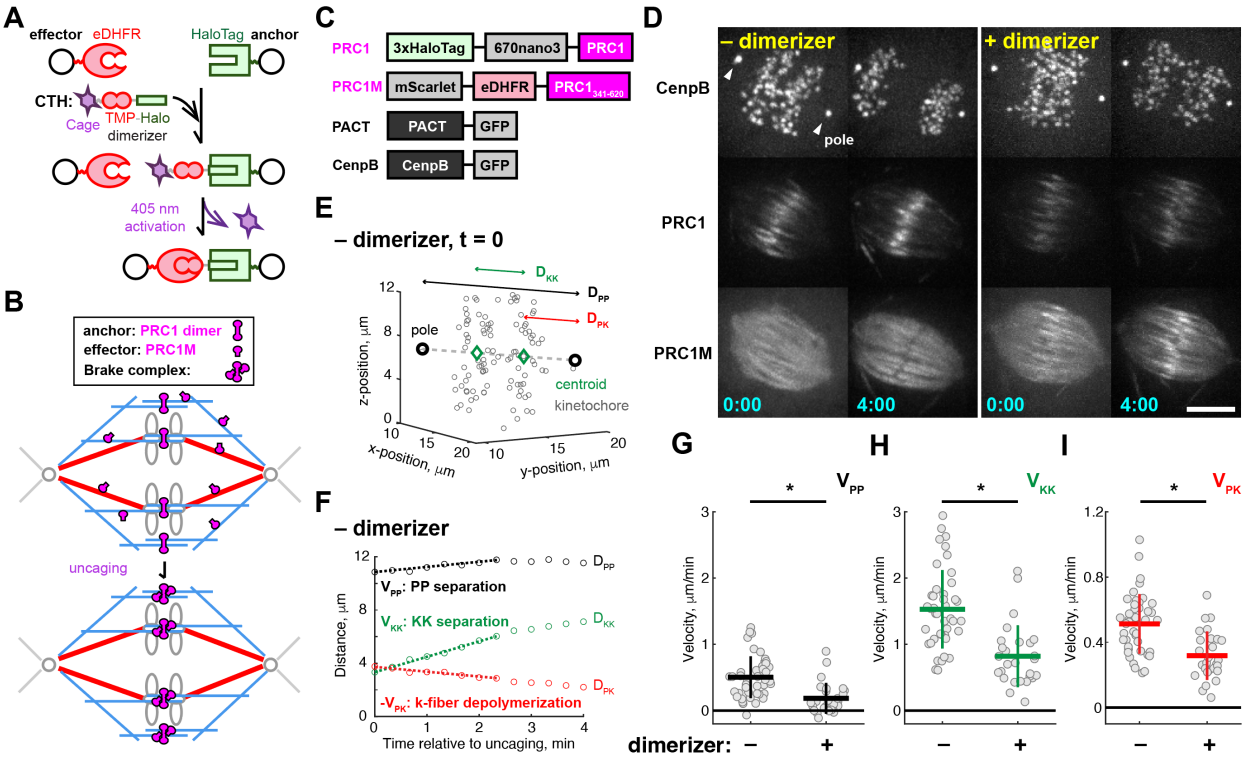

Figure 3. Suppressed bundle sliding inhibits kMT depolymerization. (A) Schematic of light-inducible dimerization. The photocaged dimerizer (CTH) includes a Halo ligand (green) linked to the eDHFR ligand trimethoprim (TMP, red) and a photocage (purple). The dimerizer is activated by uncaging to make TMP accessible to eDHFR, recruiting the eDHFR-tagged effector to the Halo-tagged anchor. **(B)** Schematic of braking assay: monomeric PRC1 (PRC1M, magenta half-dumbbells) is recruited to dimeric PRC1 (magenta dumbbells) after uncaging at t=0, forming "brake" complexes to suppress antiparallel sliding. **(C)** Constructs for braking assay. Monomeric PRC1 ($PRC1_{341\text{-}620}$) is truncated to remove the N-terminus. PACT and CENP-B label spindle poles and kinetochores, respectively. **(D)** Representative images with or without dimerization at t=0, immediately after anaphase onset. Time stamps (min:s) indicate time after uncaging at t=0. Scale bars, 5 μm. **(E-F)** Analyses of kinetochore and pole motions in anaphase. Example snapshot at t=0 (E) shows coordinates of poles (black) and kinetochores (gray circles). A pair of kinetochore centroids (green) represents the median positions of the two separating kinetochore masses projected to the mitotic axis (grey dashed lines, defined by the two poles). Three distances were calculated based on these coordinates: between kinetochore centroids (D_{KK}, green), between poles (D_{PP}, black), and between each kinetochore centroid and its adjacent pole (D_{PK}, red). Example traces (-dimerizer, F) show distances over time, with initial velocities (dashed lines) measured in the earliest time window exhibiting linear increases of all three distances. **(G-I)** Initial velocity analyses for pole separation (G), kinetochore separation (H), and kMT depolymerization (I) (n=42 cells -dimerizer and 27 cells +dimerizer). Lines: mean ± SD. *P<0.05.

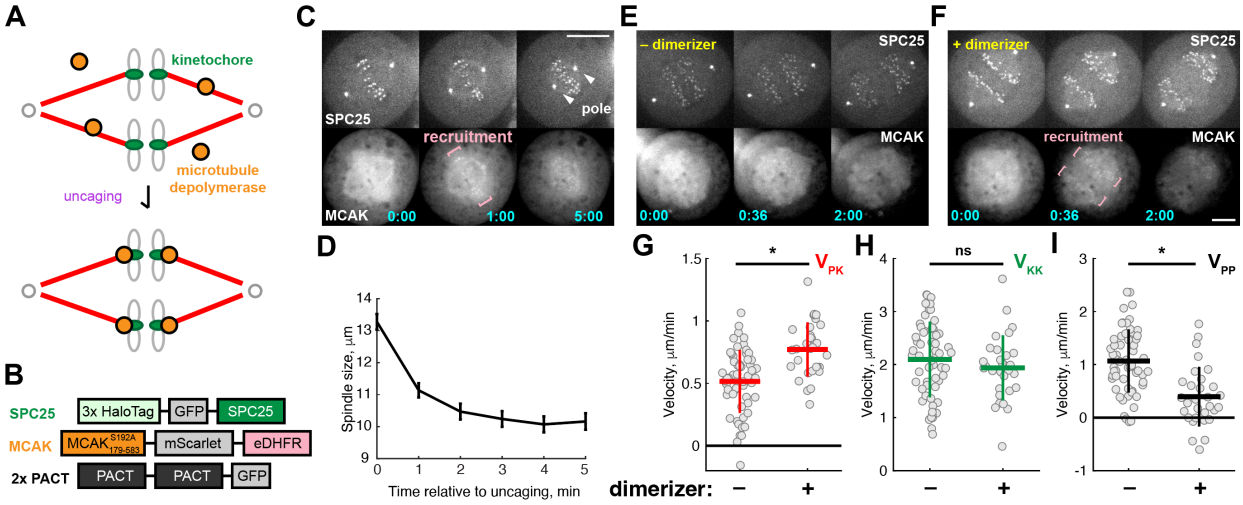

Figure 4. Enhanced kMT depolymerization slows pole separation. (A) Schematic of kMT shortening assay. The microtubule depolymerase MCAK (orange circles) is recruited to kinetochores (green ellipses) after dimerizer uncaging at t=0 to enhance kMT depolymerization. **(B)** Constructs for kMT shortening assay. The minimal microtubule depolymerization domain ($MCAK_{179\text{-}583}$) was used, with a mutation to prevent phosphorylation: S192A. SPC25 is the kinetochore anchor, and PACT labels spindle poles. **(C-D)** Metaphase kMT shortening assay. Representative images (C) show kinetochores, poles, and MCAK recruitment before and after dimerization at t=0. For each cell, pole-pole distances were measured and averaged at every time point (D, n=29 cells). Error bars: mean ± SEM. **(E-I)** Anaphase kMT shortening assay. Representative images (E-F) are shown in the presence or absence of dimerization at t=0, immediately after anaphase onset. Initial velocities for kMT depolymerization (G), kinetochore separation (H), and pole separation (I) were calculated as in Figure 3E-F (n=48 cells -dimerizer, 24 cells +dimerizer). Lines: mean ± SD. *P<0.05. Scale bars, 10 μm in C or 5 μm in F. Time stamps (min:s) indicate time after uncaging at t=0.

References

1. B. Alberts *et al.*, *Molecular Biology of the Cell*. (W. W. Norton & Company, 2022), vol. seventh edition, chap. 17, pp. 1027-1088.
2. J. M. Scholey, G. Civelekoglu-Scholey, I. Brust-Mascher, Anaphase B. *Biology (Basel)* **5**, 51 (2017).
3. K. Vukušić, I. M. Tolić, Anaphase B: Long-standing models meet new concepts. *Semin Cell Dev Biol* **117**, 127-139 (2021).
4. C. L. Asbury, Anaphase A: Disassembling Microtubules Move Chromosomes toward Spindle Poles. *Biology (Basel)* **6**, 15 (2017).
5. J. R. McIntosh, Anaphase A. *Semin Cell Dev Biol* **117**, 118-126 (2021).
6. M. I. Anjur-Dietrich, C. P. Kelleher, D. J. Needleman, Mechanical Mechanisms of Chromosome Segregation. *Cells* **10**, 465 (2021).
7. N. Pavin, I. M. Tolić, Mechanobiology of the Mitotic Spindle. *Dev Cell* **56**, 192-201 (2021).
8. J. C. Canman *et al.*, Determining the position of the cell division plane. *Cell* **424**, 1074-1078 (2003).
9. T. M. Kapoor, T. U. Mayer, M. L. Coughlin, T. J. Mitchison, Probing spindle assembly mechanisms with monastrol, a small molecule inhibitor of the mitotic kinesin, Eg5. *J Cell Biol* **150**, 975-988 (2000).
10. R. Subramanian *et al.*, Insights into antiparallel microtubule crosslinking by PRC1, a conserved nonmotor microtubule binding protein. *Cell* **142**, (2010).
11. A. Khodjakov, L. Copenagle, M. B. Gordon, D. A. Compton, T. M. Kapoor, Minus-end capture of preformed kinetochore fibers contributes to spindle morphogenesis. *J Cell Biol* **160**, 671-683 (2003).
12. R. Neef *et al.*, Choice of Plk1 docking partners during mitosis and cytokinesis is controlled by the activation state of Cdk1. *Nat Cell Biol* **9**, 436-444 (2007).
13. M. C. Pamula *et al.*, High-resolution imaging reveals how the spindle midzone impacts chromosome movement. *J Cell Biol* **218**, 2529-2544 (2019).
14. C. Mollinari *et al.*, PRC1 is a microtubule binding and bundling protein essential to maintain the mitotic spindle midzone. *J Cell Biol* **157**, 1175-1186 (2002).
15. Z. Lansky *et al.*, Diffusible crosslinkers generate directed forces in microtubule networks. *Cell* **160**, 1159-1168 (2015).
16. I. Gaska, M. E. Armstrong, A. Alfieri, S. Forth, The Mitotic Crosslinking Protein PRC1 Acts Like a Mechanical Dashpot to Resist Microtubule Sliding. *Dev Cell* **54**, 367-378.e365 (2020).
17. K. Vukušić *et al.*, Microtubule Sliding within the Bridging Fiber Pushes Kinetochore Fibers Apart to Segregate Chromosomes. *Dev Cell* **43**, 11-23.e16 (2017).
18. E. R. Ballister, C. Aonbangkhen, A. M. Mayo, M. A. Lampson, D. M. Chenoweth, Localized light-induced protein dimerization in living cells using a photocaged dimerizer. *Nat Commun* **5**, 5475 (2014).
19. H. Zhang *et al.*, Optogenetic control of kinetochore function. *Nat Chem Biol* **13**, 1096-1101 (2017).

20. G.-Y. Chen, M. A. Lampson, Chemical tools for dissecting cell division. *Nat Chem Biol* **17**, 632-640 (2021).
21. B. Orr *et al.*, An anaphase surveillance mechanism prevents micronuclei formation from frequent chromosome segregation errors. *Cell Rep* **37**, 109783 (2021).
22. K. Vukušić, I. Ponjavić, R. Buđa, P. Risteski, I. M. Tolić, Microtubule-sliding modules based on kinesins EG5 and PRC1-dependent KIF4A drive human spindle elongation. *Dev Cell* **56**, (2021).
23. G.-Y. Chen *et al.*, Tension promotes kinetochore-microtubule release by Aurora B kinase. *J Cell Biol* **220**, e202007030 (2021).
24. A. W. Hunter *et al.*, The kinesin-related protein MCAK is a microtubule depolymerase that forms an ATP-hydrolyzing complex at microtubule ends. *Mol Cell* **11**, 445-457 (2003).
25. C. H. Yu *et al.*, Central-spindle microtubules are strongly coupled to chromosomes during both anaphase A and anaphase B. *Mol Biol Cell* **30**, 2503-2514 (2019).
26. K. Laband *et al.*, Chromosome segregation occurs by microtubule pushing in oocytes. *Nature Communications* **8**, 1499 (2017).
27. A. Desai, P. S. Maddox, T. J. Mitchison, E. D. Salmon, Anaphase A chromosome movement and poleward spindle microtubule flux occur At similar rates in Xenopus extract spindles. *J Cell Biol* **141**, 703-713 (1998).
28. V. Zimyanin, S. Redemann, Microtubule length correlates with spindle length in C. elegans meiosis. *Cytoskeleton (Hoboken)*, (2024).
29. P. Suresh, A. F. Long, S. Dumont, Microneedle manipulation of the mammalian spindle reveals specialized, short-lived reinforcement near chromosomes. *Elife* **9**, (2020).
30. V. A. Valdez, L. Neahring, S. Petry, S. Dumont, Mechanisms underlying spindle assembly and robustness. *Nat Rev Mol Cell Biol* **24**, 523-542 (2023).
31. V. Sikirzhytski *et al.*, Microtubules assemble near most kinetochores during early prometaphase in human cells. *J Cell Biol* **217**, (2018).
32. F. Renda *et al.*, Non-centrosomal microtubules at kinetochores promote rapid chromosome biorientation during mitosis in human cells. *Curr Biol* **32**, 1049-1063.e1044 (2022).
33. S. Petry, A. C. Groen, K. Ishihara, T. J. Mitchison, R. D. Vale, Branching microtubule nucleation in Xenopus egg extracts mediated by augmin and TPX2. *Cell* **152**, 768-777. (2013).
34. R. Alfaro-Aco, A. Thawani, S. Petry, Biochemical reconstitution of branching microtubule nucleation. *Elife* **9**, e49797 (2020).
35. V. Štimac, I. Koprivec, M. Manenica, J. Simunić, I. M. Tolić, Augmin prevents merotelic attachments by promoting proper arrangement of bridging and kinetochore fibers. *Elife* **11**, e83287 (2022).
36. C.-K. Hu, M. Coughlin, C. M. Field, T. J. Mitchison, KIF4 regulates midzone length during cytokinesis. *Curr Biol* **21**, 815-824 (2011).

37. P. Kunchala *et al.*, Plasticity of the mitotic spindle in response to karyotype variation. *Curr Biol* **34**, 3416-3428.e3414 (2024).
38. C. Arquint, A.-M. Gabryjonczyk, E. A. Nigg, Centrosomes as signalling centres. *Philos Trans R Soc Lond B Biol Sci* **369**, 20130464 (2014).
39. T. D. Pollard, Nine unanswered questions about cytokinesis. *J Cell Biol* **216**, 3007-3016 (2017).
40. S. Dumont, T. J. Mitchison, Force and Length in the Mitotic Spindle. *Curr Biol* **19**, R749-R761 (2009).
41. P. Khandelia, K. Yap, E. V. Makeyev, Streamlined platform for short hairpin RNA interference and transgenesis in cultured mammalian cells. *Proc Natl Acad Sci U S A* **108**, 12799-12804 (2011).
42. P. D. Andrews *et al.*, Aurora B regulates MCAK at the mitotic centromere. *Dev Cell* **6**, 253-268 (2004).
43. R. Subramanian, S.-C. Ti, L. Tan, S. A. Darst, T. M. Kapoor, Marking and measuring single microtubules by PRC1 and kinesin-4. *Cell* **154**, 377-390 (2013).
44. A. K. Gillingham, S. Munro, The PACT domain, a conserved centrosomal targeting motif in the coiled-coil proteins AKAP450 and pericentrin. *EMBO Rep* **1**, 524-529 (2000).

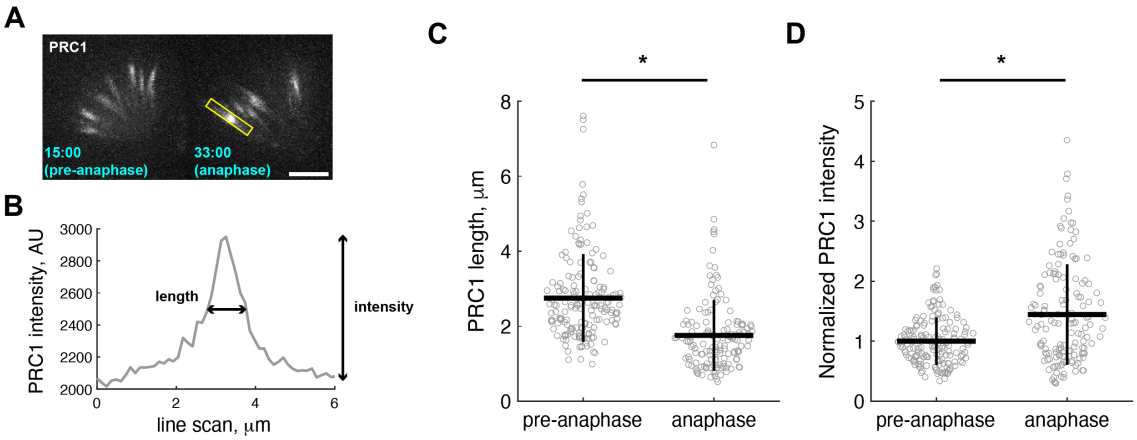

Figure S1. PRC1 morphology in monopolar spindles. (A) Representative images of PRC1 bundles before (left) or after (right) anaphase onset. Time stamps indicate the time after uncaging. Scale bars, 5 μm. **(B)** An example of PRC1 intensity analyzed by line scan (box in A). Bundle length and intensity are defined by the full width at half-maximum and the peak height, respectively. **(C-D)** Analyses for bundle length (C) and intensity (D). Each dot represents a PRC1 bundle (N = 162 for pre-anaphase bundles and 148 for anaphase bundles from 23 cells). Lines: mean ± SD. *P<0.05.

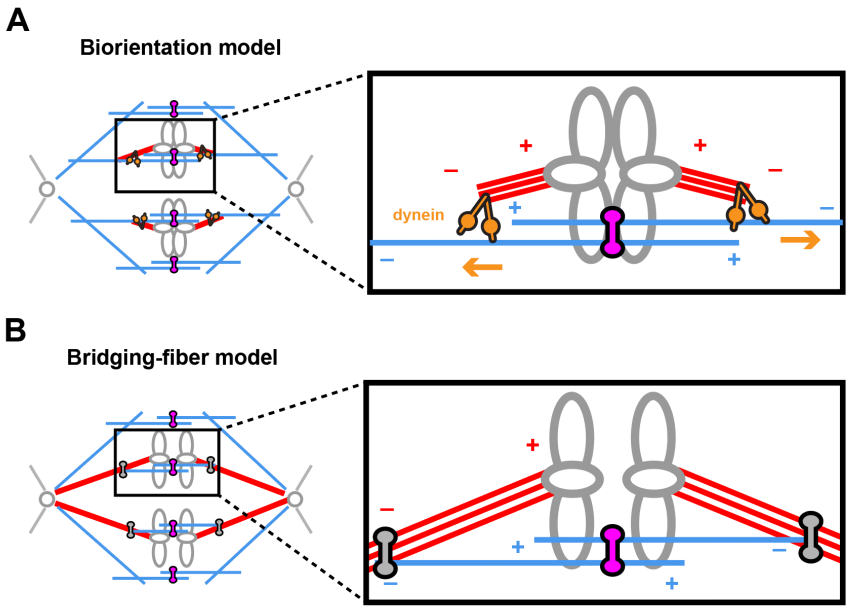

Figure S2. Proposed mechanisms of parallel coupling. (**A**) Kinetochore-nucleated kMT fragments (red) have their plus-ends at kinetochores. Dynein motors at the minus-ends of these short kMTs preferentially guide kMT growth towards the minus ends of parallel microtubules in the central spindle (blue). (**B**) A fraction of the central spindle is grown by microtubules branching from kMTs (via augmin complexes and NuMA). These branching microtubules (blue) form antiparallel bundles (bridging fibers) between the two sister kinetochores, bound by antiparallel crosslinkers (magenta).

Video 1. Max-intensity projection over 2 μm showing the off-bundle sister kinetochore pair (yellow arrow) indicated by the gray box in Figure 2B. Time stamps (min:s) indicate time after uncaging at t=0. Scale bar: 5 μm.

Video 2. Max-intensity projection over 2 μm showing the on-bundle sister kinetochore pair (yellow arrow) indicated by the green box in Figure 2B. Time stamps (min:s) indicate time after uncaging at t=0. Scale bar: 5 μm.

Video 3. Max-intensity projection over the whole cell for the cells shown in Figure 3D. Left: - dimerizer; Right: + dimerizer. Time stamps (min:s) indicate time after uncaging at t=0. Scale bar: 5 μm.

Video 4. Max-intensity projection over 1 μm for the cell shown in Figure 4C. Time stamps (min:s) indicate time after uncaging at t=0. Scale bar: 10 μm.

Video 5. Max-intensity projection over 4 μm for the cells shown in Figure 4E-F. Left: Figure 4E; Right: Figure 4F. Time stamps (min:s) indicate time after uncaging at t=0. Scale bar: 5 μm.